Surface Science Reports 75 (2020) 100482

Contents lists available at ScienceDirect

Surface Science Reports

journal homepage: www.elsevier.com/locate/surfrep

Wettability of graphene

Liubov A. Belyaeva, Grégory F. Schneider*

Leiden University, Faculty of Science, Leiden Institute of Chemistry, Einsteinweg 55, 2333CC, Leiden, the Netherlands

ARTICLE INFO

Article history:
Received 31 October 2019
Received in revised form
29 January 2020
Accepted 16 March 2020
Available online 20 March 2020

ABSTRACT

Many far-reaching applications of graphene require a deep understanding of the interactions between graphene and other surfaces, including the wetting behaviour of graphene. However, its two-dimensional nature does not allow qualifying graphene as simply hydrophobic or hydrophilic, but instead gives rise to a diversity of interfacial phenomena governing the apparent wettability of graphene. As a result, wide disparities in the wetting properties of graphene have been widely reported. In this review we analyse the wettability of graphene with a special focus on the experimental conditions and on discriminating the causes of the reported inconsistencies. The elimination of the environmental factors causing misleading data is a major challenge. Importantly, progresses made in graphene research yielded new experimental insights and tools enabling the minimization of unwanted effects and, ultimately, the achievement of reliable contact angle measurements. Besides the macroscopic wettability studied using contact angle measurements under ambient conditions or by theoretical modelling, we also analysed correlations with the wettability of graphene at the molecular level in supremely pure environment of ultra-high vacuum.

Contents

1. Introduction

The wettability of a solid surface characterizes its affinity to water and provides an indication about possible interactions with molecules other than water [1,2]. For graphene, however, a simple measurement of the water contact angle yielded a remarkably wide range of values – from hydrophilic [3,4] to hydrophobic [5–9] – and an extensive debate over the origin of the contact angle discrepancies, which still seems not resolved. Most researchers now agree that, due to the atomic thickness of graphene, the underlying substrate has a critical effect on the apparent wettability of graphene [7,10–14]. On the other hand, the extent to which graphene is transparent to wetting is still debated – graphene has been reported to be fully wetting transparent [10], partially wetting transparent [13,15,16] and fully opaque [7,8,17]. The apparent (i.e. observed experimentally) wettability of graphene is determined by the intrinsic wettability of graphene and external factors impacting this wettability. The intrinsic wettability of graphene is dictated solely by the properties of pristine and isolated graphene, a

* Corresponding author.
E-mail address: g.f.schneider@chem.leidenuniv.nl (G.F. Schneider).

https://doi.org/10.1016/j.surfrep.2020.100482

situation which does not occur practically. All external factors altering the intrinsic wettability of graphene can be categorized into 1) fundamental substrate effects and 2) environmental effects. Fundamental substrate effects include well-defined (as opposed to environmental) effects of the polarity [18] and doping of the substrate [19,20]. In principle, the intrinsic wettability and the substrate effects are sufficient to describe the wettability of supported graphene. They are, however, often hindered by the environmental effects, which are induced un-intentionally during sample preparation (polycrystalline graphene samples with different size and orientation of domains [21,22], transfer and handling-related contamination and structural irregularities [23]) and by measurement conditions (adsorption of air contaminants [15,24]). Environmental factors do not represent the properties of graphene, nor of the substrate, and often cause non-negligible sample-to-sample variations and, therefore, must be minimized [24]. In practice, however, the contributions of the substrate and of the environment are difficult to disentangle. The following subchapters will introduce the intrinsic wettability of graphene, and discuss how wettability is affected by the substrate and the environment.

In addition to the conventional characterization of wettability in ambient by means of contact angle measurements, interactions between graphene and other molecules in ultra-high vacuum (UHV) can also be investigated using surface science methods [25–31]. For example, comparing UHV and ambient studies demonstrated that the microscopic hydrophobicity does not straightforwardly translate into macroscopic hydrophobicity, but rather provides complementary insights.

1. Thermodynamics of graphene wetting

The surface energy of a solid σ_S, is the interfacial tension of a solid-gas interface σ_{SG}, and is defined as an excess energy of its surface compared to the bulk, and is related to the contact angle θ with the Young equation (Fig. 1a):

$$\sigma_{SG} - \sigma_{SL} - \sigma_{LG}\cos\theta = 0$$

where σ_{SL} is solid-liquid interfacial energy and σ_{LG} is liquid-gas interfacial energy (or surface tension of the liquid σ_L).

Graphene and other two-dimensional (2D) materials do not have a bulk phase, and, therefore, the definition of the surface energy cannot be applied to describe a completely isolated monolayer graphene. The contact angle and the surface energy of graphene, therefore, must be always regarded in the context of the underlying substrate (or liquid and gaseous medium underneath graphene). In fact, similarly to the water contact angle measurements, attempts to determine the surface energy of graphene resulted in very sparse and spreaded values. As a few examples, the surface energy was reported to be 46.7 mJ/m^2 for graphene on a silicon substrate (chemically exfoliated flakes) [32], 62.2 ± 3.1 mJ/m^2 for graphene on copper (CVD) [15], 40.4 mJ/m^2 for graphene on PDMS (CVD) [13], 48.8 mJ/m^2 for graphene on glass [13] and 115 ± 4 mJ/m^2 for suspended graphene (CVD) [33]. These examples demonstrate that the deviations from the structurally ideal non-contaminated graphene surface, caused by environmental factors (production method, transfer, environment) and by the effect of the underlying substrate, result in graphene interfaces with significantly different wetting properties. Table 1 summarizes reported water contact angle and surface energy values determined experimentally for monolayer graphene with regard to its crystallinity (mono- or polycrystalline), production, transfer methods, and methods used to calculate the surface energy. Theoretical studies also show disagreement: molecular dynamic (MD) simulations predict a surface energy of zero [34], whereas quantum Monte Carlo and advanced density-functional first-principles calculations predict values in the range 144–171 mJ/m^2 [35,36].

The type of interactions between graphene and a wetting liquid can be determined from the contributions of polar (hydrogen bonding, dipole-dipole and dipole-induced dipole) and dispersive (London-van der Waals) interactions to the total surface energy [37], by measuring multiple contact angle measurements with liquids of different polarities as described in Fowkes [38], Owens-Wendt [39] or Neumann models (Fig. 1) [40–42]. Interestingly, such an approach yielded more consistent results than determining the total surface energy (i.e. the sum of dispersive and polar contributions): most studies agree, in qualitative terms, on the dominance of the dispersion forces in the surface energy of graphene [3,13,15,18,43]. Moreover, by comparing polar (σ_S^P) and dispersive (σ_S^D) components of graphene-on-a-substrate (σ_{S2}^D and σ_{S2}^P in Fig. 1c) and those of the bare substrate (σ_{S1}^D and σ_{S1}^P in Fig. 1c), the transmittance of graphene to specific interactions (polar or dispersive) can be estimated (Fig. 1c) [3,13], providing new insights into the chemical origin of the wetting transparency of graphene. In the case of a clean non-corrugated graphene-substrate interface (i.e. when the interface is not exposed to air and is not subjected to any transfer-related contamination and mechanical deformation) the graphene was transparent to both polar and dispersive interactions independently of the polarity of the substrate. In contrast, when it was transferred on a substrate using the widely-used polymer-assisted method, graphene was almost entirely opaque to polar interactions, presumably due to contamination and morphological distortions (Fig. 1d) [3,44]. This hypothesis agrees with a separate study, where graphene was transferred to six different substrates and where – for all samples – the polar component was screened by graphene while the dispersive component increased [13].

2. Wetting of free-standing graphene

The characterization of the intrinsic wetting properties of graphene is technically complicated, because both the environmental factors and the substrate contribute to the observed wetting characteristics. The influence of the substrate can be eliminated in a free-standing geometry. However, so far, it was only possible to make graphene free-standing over a few square micrometers, rendering difficult to measure the contact angle of a microliter droplet (with a millimeter-range diameter). Simulations of the contact angle of water on free-standing graphene have been challenging as well and were shown to highly depend on the choice of the graphene-water interaction model. Suchwise, independent MD simulations resulted in contact angles for suspended graphene as different as 90–127° [7,50,51] and 45.7°±1.3° [52].

Only a few experimental approaches attempting to circumvent the complications of the conventional contact angle measurements yielded information on the intrinsic wettability of suspended graphene [4,6,49]. In the first study, graphene was suspended over hydrophilic and hydrophobic nanopatterned silicon substrates (Fig. 2a) with varying area fractions of suspended graphene. By extrapolation of the contact angle values of partially suspended graphene, the water contact angle for fully suspended graphene was estimated to be 85°±5°. Interestingly, the contact angle of partially suspended graphene did not depend on the area of suspended graphene (i.e. it was 85°±5° for all measured area fractions, Fig. 2b), and neither on the wettability of the underlying substrate (Fig. 2b) [49]. The major drawback of using partially suspended graphene is that the deposition of monolayer graphene on such sharply patterned structures (the conical pillars were 5–15 nm in width, spaced by ~50 nm, Fig. 2a) and the water-based transfer method that was used, created a large density of wrinkles, pinholes and cracks which certainly altered the structural properties of the

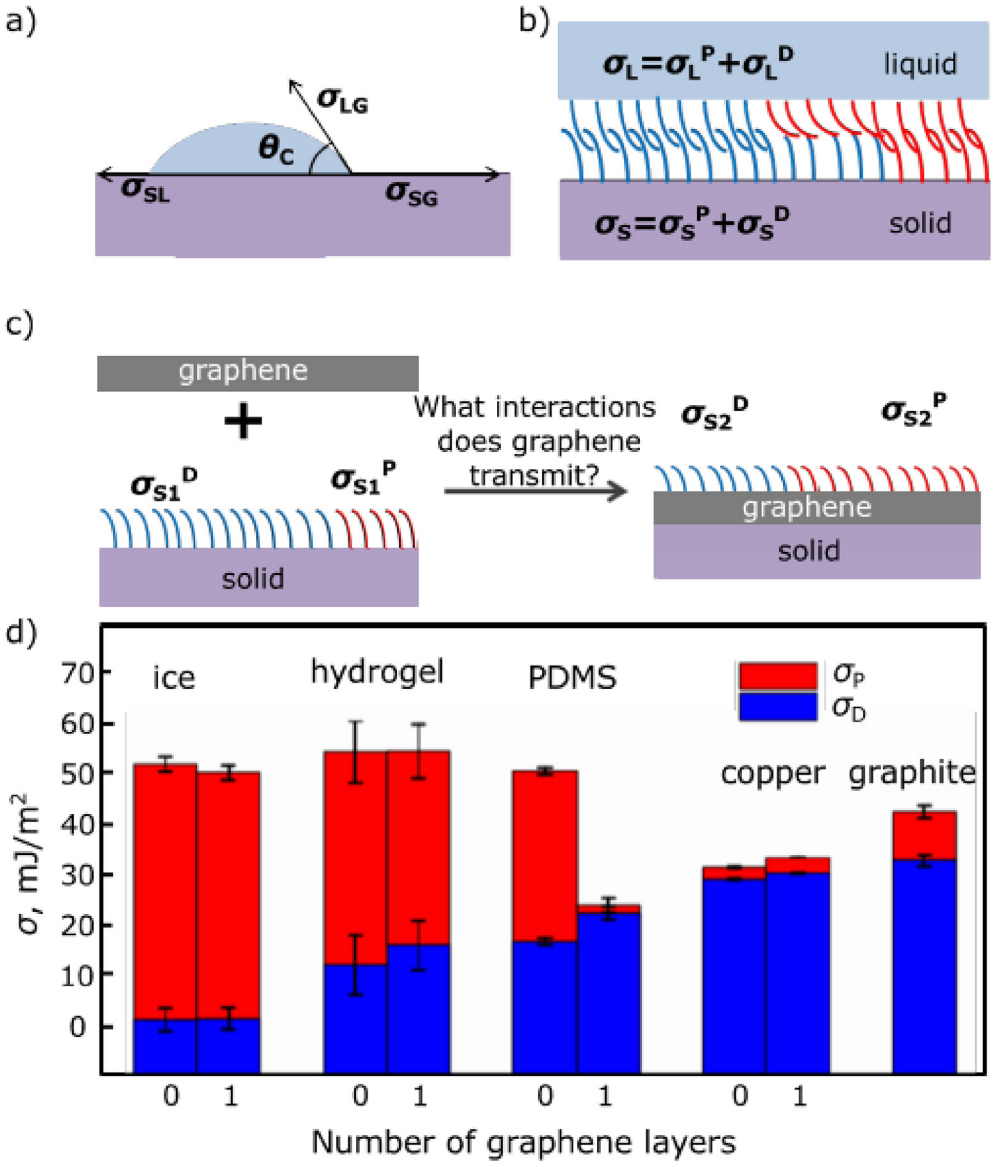

Fig. 1. Contact angle measurements and wetting transparency. a) Three phase equilibrium diagram in the sessile drop technique: θ_C is the contact angle and σ_{SL}, σ_{LG} and σ_{SG} are the interfacial tensions at the solid-liquid, liquid-gas and solid-gas interfaces respectively. b) Illustration of polar and dispersive interactions between a solid and a liquid represented by the polar (σ_S^P and σ_L^P) and dispersive (σ_S^D and σ_L^D) components of the surface tensions σ_S and σ_L. Blue and red lines depict the contributions of dispersive and polar interactions respectively. c) Illustration of the effect of graphene transmitting polar and dispersive components of the surface energy of the solid substrate. The addition of a graphene layer on top of the solid changes the contributions of polar and dispersive interactions from σ_{S1}^D and σ_{S1}^P to σ_{S2}^D and σ_{S2}^P. d) Polar and dispersive components of the surface energy of graphene on ice, hydrogel, polydimethylsiloxane (PDMS) and copper compared with the surface energies of the bare substrates [3]. (For interpretation of the references to colour in this figure legend, the reader is referred to the Web version of this article.)

graphene surface [49]. Moreover, the ability of such suspended graphene structures to sustain the weight of a water droplet, particularly for contact angle measurement, was not supported experimentally and is, therefore, questionable.

In a second study, the wetting properties of suspended graphene were characterized based on the ability of graphene nanopowders to absorb water [6]. Graphene nanopowders consisted of nanoflakes of reduced graphene oxide separated by air cavities and, therefore, represented free-standing graphene. Remarkably, water adsorption measurements on such graphene nanopowders of different thicknesses (i.e. flakes of different number of stacked graphene monolayers) yielded contact angles of 179°±2° (for nanopowders with monolayer flakes), 163°±2° (for nanopowders with the flakes of 4–5 layers) and 140°±2° (for nanopowders with the flakes of 25 layers) [6]. The "liquid marbles" experiments, in which the ability of a powder to adsorb on a water droplet is tested, also showed that the nanopowder composed of monolayer flakes is superhydrophobic (no flakes adsorbed on the surface of the droplet, Fig. 2c) while nanopowder samples with 4–5 layers flakes showed a hydrophobic character (the flakes indeed adsorbed on the surface of the droplet, without intruding inside the droplet, Fig. 2c). Although the experimental approach was clever from a methodological point of view, reduced graphene oxide powders are, however, different from pristine graphene monolayer as they are structurally disordered materials containing significant amount of oxidized edges (based on Raman spectroscopy and chemical analysis) particularly the powder containing the thinnest flakes (~one layer).

In addition, besides still being indirect indications of the wettability of free-standing graphene, the two approaches

Table 1
Experimental water contact angle and surface free energy values of monolayer graphene on different substrates.

Substrate	Type of graphene	Transfer method	Contact angle, °	Surface energy, J/m^2	Method used to determine the surface energy	Ref.
Cu	Polycrystalline CVD	As-grown	86.2	–		10
	Polycrystalline CVD (fresh)	As-grown	44	–		24,45
	Polycrystalline CVD (aged)	As-grown	80	–		24
	Polycrystalline CVD (fresh)	As-grown	47–53	62.2 ± 3.1	Fowkes theory	15
				53.0 ± 4.3	Owens-Wendt theory	
				63.8 ± 2.0	Neumann's theory	
	Polycrystalline CVD (aged)	As-grown	70–83	45.6 ± 3.9	Fowkes theory	15
				37.5 ± 2.3	Owens-Wendt theory	
				57.4 ± 2.1	Neumann's theory	
	Polycrystalline CVD (aged)	As-grown	80	–		19
	Polycrystalline CVD	As-grown	~81	–		20
	Polycrystalline CVD	As-grown	80 ± 5	43.0	Owens-Wendt theory, based on CA measurements	3
	Polycrystalline CVD (fresh)	As-grown	~61	~48	Adjusted van Oss–Chaudhury–Good model, based on CA measurements	46
	Polycrystalline CVD (aged)	As-grown	~92	39–40	Adjusted van Oss–Chaudhury–Good model, based on CA measurements	46
	Single-crystal CVD	As-grown	91	–		47
Ni	Polycrystalline CVD (fresh)	As-grown	~85	~44	Adjusted van Oss–Chaudhury–Good model, based on CA measurements	46
	Polycrystalline CVD (aged)	As-grown	~98	39–40	Adjusted van Oss–Chaudhury–Good model, based on CA measurements	46
SiO_2/Si	Polycrystalline CVD	PC-assisted	77.7	41	Owens-Wendt theory, based on CA measurements	13
	CVD	PMMA-assisted	88	–		19
	Polycrystalline CVD	Polymer-free	78–81	–		20
	Chemically exfoliated rGO	No transfer	127 ± 4	46.7	Neumann's theory, based on CA measurements	32
	Polycrystalline CVD	PMMA-assisted	86.3	34.68	Owens-Wendt theory, based on CA measurements	43
	Polycrystalline CVD (right after annealing)	Not specified	60 ± 3	–		45
h-BN/SiO_2/Si	Polycrystalline CVD	PMMA-assisted	79.1	36.69	Owens-Wendt theory, based on CA measurements	43
SiC	Epitaxial	As-grown	92.5	–		17
PDMS	Polycrystalline CVD	Direct adhere	105.1	40.4	Owens-Wendt theory, based on CA measurements	13
	Polycrystalline CVD	Bubbling method	92	–		48
	Polycrystalline CVD	Polymer-free	91 ± 1	35 ± 2	Owens-Wendt theory, based on CA measurements	3
Oxidized PDMS	Polycrystalline CVD	Direct adhere	69.5	31.6	Owens-Wendt theory, based on CA measurements	13
Glass	Polycrystalline CVD	PC-assisted	70	48.8	Owens-Wendt theory, based on CA measurements	13
	Polycrystalline CVD	Bubbling method	~60	–		48
	Polycrystalline CVD	PMMA-assisted	48.1	–		10
Si	Polycrystalline CVD	PC-assisted	83.2	38.4	Owens-Wendt theory, based on CA measurements	13
	Polycrystalline CVD	Bubbling method	~70	–		48
	Polycrystalline CVD	PMMA-assisted	33.2	–		10
Al_2O_3	Polycrystalline CVD	PC-assisted	75.4	42	Owens-Wendt theory, based on CA measurements	13
Au	Polycrystalline CVD	PMMA-assisted	78.8	–		10
Ru(0001)	Single-crystal epitaxial	As-grown	~98	–		9
Water ice (0 °C)	Polycrystalline CVD	No transfer	30 ± 5	60 ± 1	Owens-Wendt theory, based on CA measurements	3
Water hydrogel	Polycrystalline CVD	No transfer	10 ± 2	63 ± 5	Owens-Wendt theory, based on CA measurements	3
Free-standing*						
*partially suspended	Polycrystalline CVD	Polymer-free	85 ± 5	–		49
*liquid marble	Chemically-exfoliated rGO	No transfer	180	–		6
*captive bubble	Polycrystalline CVD	No transfer	42 ± 3	–		4
	Polycrystalline CVD	PS-assisted	–	115 ± 4	Surface force apparatus and JKR theory	33

described above do not take into account the adsorption of airborne hydrocarbons which are known to substantially alter the wetting of graphitic surfaces [24,53,54].

In contrast, the direct contact angle measurement on fully free-standing graphene, realized by captive bubble method, revealed the intrinsic hydrophilicity of graphene monolayer, with a contact angle of 42°±3°, i.e. equal to that of clean freshly-exfoliated graphite [4]. The captive bubble method is, in essence, an inverse equivalent of the sessile drop method, where instead of the contact angle of a water drop on top of free-standing graphene, the contact angle of an air bubble underneath graphene immersed in water is measured (Fig. 2d) [55,56]. Remarkably, such design provides measurements on large area of smooth (i.e. graphene floats on the surface of water) fully free-standing graphene and avoids any transfer-related contamination and adsorption of hydrocarbons [24].

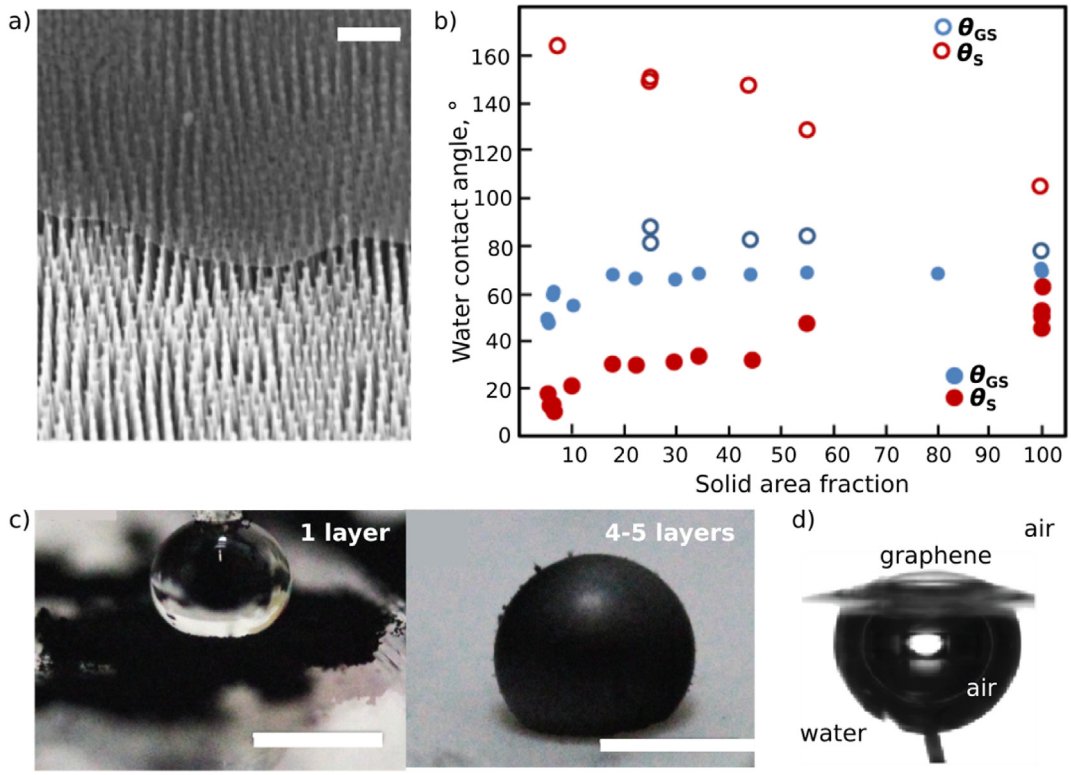

Fig. 2. Experimental water contact angle measurements on free-standing graphene. a) Scanning Electron microscopy (SEM) image of a graphene monolayer partially suspended over nanopatterned silicon pillars [49]. The scale bar represents 200 nm. b) Contact angle as a function of solid area fraction at the top of the texture [49]: water contact angle values for bare hydrophilic pillars (θ_S) are represented by filled (hydrophilic) red circles, for bare hydrophobic pillars – by hollow red circles; water contact angle values for graphene deposited on hydrophobic and hydrophilic substrates (θ_{GS}) are represented by hollow and filled blue circles respectively. c) Graphene (reduced graphene oxide) nanopowders of monolayer (left) and 4–5 layers (right) flakes in contact with a water droplet, i.e. the "liquid marble"experiment [6]. The scale bars represent 2 mm. d) The captive bubble design for water contact angle measurements on free-standing graphene: an air bubble is injected underneath a graphene layer floating on the surface of water [4]. (For interpretation of the references to colour in this figure legend, the reader is referred to the Web version of this article.)

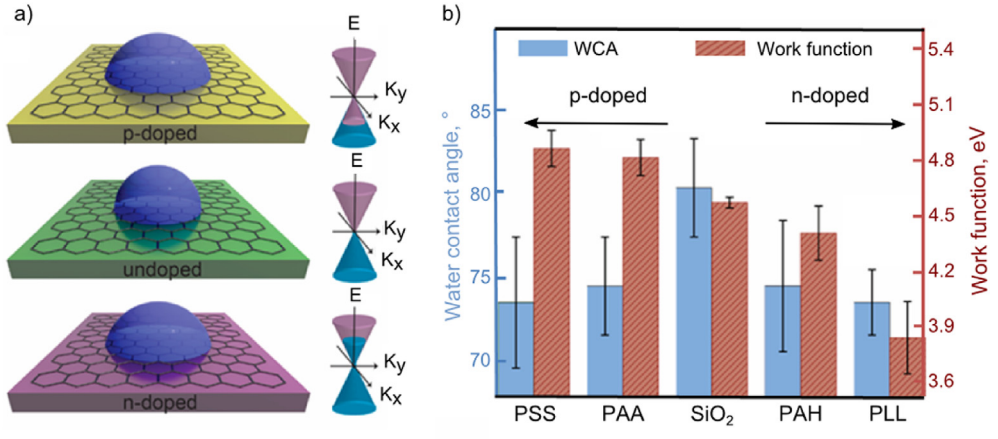

Fig. 3. Effect of doping on the water contact angle of graphene. a) Illustration of the effect of the doping-induced shift of the Fermi level of graphene on the measured water contact angle [20]. b) Water contact angle and work function of undoped graphene on a SiO_2 substrate and for graphene doped by introducing a layer of poly(sodium 4-styrenesulfonate) (PSS), poly(acrylic acid) (PAA), poly(allylamine hydrochloride) (PAH) and poly-L-lysine (PLL) between graphene and the SiO_2 substrate [20].

3. Effects of the substrate on the wettability of graphene

The substrate on which graphene is transferred or grown has a strong influence on the wettability of graphene. In fact, the underlying substrate alters the electronic structure and, consequently, the chemical potential of graphene. The first MD modelling of van der Waals (vdW) interactions between a liquid and a graphene sheet introduced the "wetting translucency" as opposed to the "wetting transparency" of graphene and suggested that wetting transparency does not occur when graphene is supported by superhydrophobic or superhydrophilic substrates [12]. The model, however, assumes that the solid-liquid interactions are dominated

by vdW forces and does not take into account the electrostatic interactions or hydrogen bonding between liquids and solids, which could also contribute to the wetting properties.

Interestingly, density-functional theory (DFT) calculations showed that the dipole moment of water does not affect the electronic structure and doping in fully suspended graphene [5,57]. However, if a solid substrate is present (namely, SiO_2 [57] and copper [18]), the subsequent charge transfer between the substrate and the graphene triggers the polarization effect of water on graphene [57] and modulates the Fermi level of graphene [18,58], all of which result in altering the graphene-water interactions and, therefore, the apparent macroscopic wettability.

Finally, experimental studies also confirmed that inducing p- or n-doping by applying a gate voltage (Fig. 3a) [19], or by introducing a layer of metal or polyelectrolytes (namely poly(sodium 4-styrenesulfonate), poly(acrylic acid), poly(allylamine hydrochloride) and poly-L-lysine) between graphene and the substrate, or fabricating metal-graphene heterojunctions [20], alters the properties of graphene towards more hydrophilic (Fig. 3b) [19,20]. According to DFT and atomistic calculations, the induced doping modulates the charge carrier density in graphene and the binding energy between graphene and water, which – in turn – affects the wettability of graphene [20].

4. Environmental factors affecting the wettability of graphene

Environmental factors are the factors responsible for the variability of reported contact angles due to sample preparation and measurement conditions (adsorption of airborne hydrocarbons, growth and transfer of graphene).

The adsorption of airborne hydrocarbons is the major cause of the false apparent hydrophobicity of graphitic surfaces and errored contact angle of ~90° [24,46,52,54,58–61]. In fact, ellipsometry and attenuated total reflectance-Fourier transform infrared spectroscopy (ATR-FTIR) studies showed that a 5 Å thick layer of hydrocarbon contaminants forms on graphite upon exposure to air [62]. Disproving the long-held belief, first, graphite [53], and then graphene [15,24] were demonstrated to be intrinsically mildly hydrophilic exhibiting contact angles of ~60° and ~40° (for graphene on copper) respectively, when the measurements were conducted on contamination-free samples (Fig. 4a). Hydrocarbons are ubiquitously present in the environment. Important to highlight that storing graphene samples in a plastic Petri dish as opposed to a glass one results in a noticeable increase of the contact angle in the course of 15 min (Fig. 4b) [24]. Thermal annealing, ultraviolet ozone treatment [24] and hydrogen plasma [63] can be utilized to remove the adsorbed hydrocarbons from graphene (Fig. 4c). Another way to preserve the intrinsic wettability of graphene is to store graphene at low temperature (−15 °C): a protective layer of water forms on the graphene surface preventing hydrocarbon adsorption [45]. Contact angle measurements (and any other surface inspection) on graphene samples must, therefore, be conducted within minutes after growth or using the surface treatments mentioned above.

Separately, the broad diversity of synthetic [21] and transfer [23] methods yield graphene materials with different surface properties [22,64]. Most wettability studies were performed on CVD grown graphene, as CVD is the most convenient method to produce large sheets of monolayer graphene up to now, suitable for contact angle measurements [65–71]. However, even considering only CVD graphene samples, varying the growth conditions (catalytic metal, morphology of the substrate, temperature, pressure, annealing conditions, precursor gas, gas flow, presence of oxygen and hydrogen) results in different number of layers, domain size and orientation, type and density of defects, density of oxidized carbon atoms, size and density of wrinkles and other morphological features, which affect the wetting behavior of graphene [72]. For example, the introduction of point defects in the graphene lattice using an oxygen plasma changed the contact angle of graphene on SiC from 92.5° to 55.1°, and the subsequent restoration of the graphene lattice upon annealing in UHV increased the contact angle to 87.3°, close to the pristine value [17]. Important to note that most studies probed the wettability of polycrystalline CVD graphene, while there are only few works reporting contact angles measured

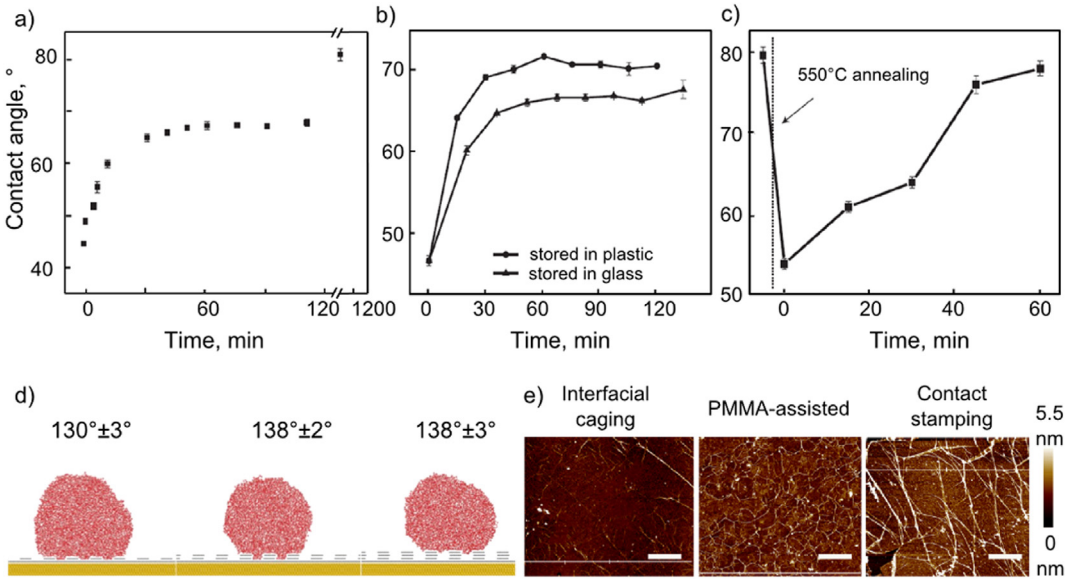

Fig. 4. Environmental effects affecting the wettability of graphene. a) Water contact angle of monolayer graphene-on-copper upon exposure to ambient air after CVD growth [24]. b) Water contact angles of graphene-on-copper stored in plastic and glass Petri dishes as a function of storage time [24]. c) Effect of annealing at 550 °C in argon atmosphere on the water contact angle of graphene on copper [24]. d) MD simulation of the effect of surface morphology on the water contact angle of graphene [74]. e) AFM images of wrinkles, folds, contamination and other imperfections in graphene transferred on a Si/SiO_2 substrate using the interfacial caging, PMMA-assisted and contact stamping transfer methods [76]. The scale bars represent 2 μm.

on single-crystalline graphene: ~98° for epitaxially-grown graphene on ruthenium [9] and 91° for CVD-grown graphene on copper [47]. The possible alteration of the wettability that the grain boundaries may induce is not fully understood yet, with only few indications on the interactions between a single grain boundary and the adsorbate molecule [73]. Specifically, scanning tunnelling microscopy (STM) showed that interactions between water and line defects (dislocations and grain boundaries) caused water to intercalate and split the graphene into fragments [73]. Interestingly, this phenomenon was shown to be substrate-dependent and was observed for graphene on Ru(0001) but not on Cu(111), with copper known to interact more weakly with graphene [73]. Also, a number of MD studies reported that the imperfections in graphene, such as multilayers [74], holes [75] and roughness [16,74] generate a variety of wetting states (Fig. 4d), naturally implying that varying their concentrations and dimensions would result in different wettabilities.

Yet, the transfer of graphene from the growth catalyst to a target substrate induces even larger irregularities (ripples, folds, cracks, contamination) in the graphene structure and graphene-substrate interface, and causes additional sample-to-sample variations (Fig. 4e) [62,72]. The most widely used polymer-based transfer methods irreversibly contaminate the surface with polymer residues (Fig. 4e) [77,79–81], whereas alternative polymer-free transfer methods provide minimal contamination [82–86], often at the cost of disintegrity and formation of micrometer-sized folds and wrinkles in the graphene layer [76,87]. A comparative study of three types of samples (non-transferred graphene samples, graphene transferred using a polymer-free method and samples transferred using PMMA) pinpointed an interesting trend: the non-transferred graphene samples were transparent to wetting, graphene transferred using a polymer-free method significantly altered the contact angle and surface energy of the substrate, and samples transferred using PMMA yielded irreproducible wetting behavior, suggesting that transfer, contamination and handling yield graphene with large sample-to-sample variation from very hydrophilic to hydrophobic [3]. The same conclusion was made by comparing the surface energy of a pristine exfoliated flake with that of CVD graphene transferred with the PMMA-assisted method [44].

5. Microscopic wettability of graphene

In parallel with the macroscopic investigations in ambient atmosphere, surface science methods were also employed to probe the affinity of water molecules to graphene under UHV conditions, the so-called “microscopic wettability” or wettability at the molecular level [25–31,88–90]. Measurements under UHV provide an extreme purity of the environment and sensitivity and can, in principle, allow the accurate probing of the interactions between graphene and single water molecules. Temperature programmed desorption (TPD) is a method typically used for investigating the microscopic wettability of surfaces [91]. Essentially, a TPD experiment yields a desorption curve which represents the amount of water molecules (or of other adsorbate) desorbing from a surface upon heating. Typically, a set of curves is recorded at different initial partial pressures of water in the UHV chamber (that is, different coverages of the studied surface with water). The onset temperature at which molecules start desorbing, the shape of the curves and the evolution of the curves with increasing coverage (alignment of the leading edges, tails etc.) provide information about the desorption energy, the kinetic order of desorption, the binding energy and the ordering of the adsorbate molecules in the first and subsequent adsorbate layers [91].

It must be noted, however, that the wettability at the molecular level cannot be directly compared with the macroscopically observed wettability, as experimental conditions are different (i.e. UHV versus ambient) and TPD studies refer to different molecular events (i.e. the adsorption of single molecules versus a collective adsorption of molecules in contact angle measurements). The difference between desorption and reaction mechanisms in UHV and ambient atmosphere, the so-called “pressure gap”, is an interesting subject on its own, and most recent advances in understanding its physical nature can be found elsewhere [92].

A number of thorough studies reported on the desorption kinetics of water [27], methanol [27], ethanol [27], Ar [29], Kr [29], Xe [29], N_2 [29], O_2 [29], CO [29], methane [29], ethane [29], propane [29], benzene [30] and cyclohexane [30] from graphene grown on Pt(111) *in situ* in a UHV chamber. Interestingly, while most adsorbates showed kinetics orders and desorption energies very similar to those on highly oriented pyrolitic graphite (HOPG) [93], water displayed a more complicated behaviour at submonolayer coverages (i.e. when the amount of water molecules is not enough to form a continuous monolayer): misaligned leading edges, “dips” and “bumps”, peak shifts to higher temperatures upon desorption of the second and subsequent layers. It was reported that the first monolayer of water forms a new ice polymorph on graphene, in which planar hexagons of water molecules are stacked directly on top of each other, maximizing the number of hydrogen bonds (at

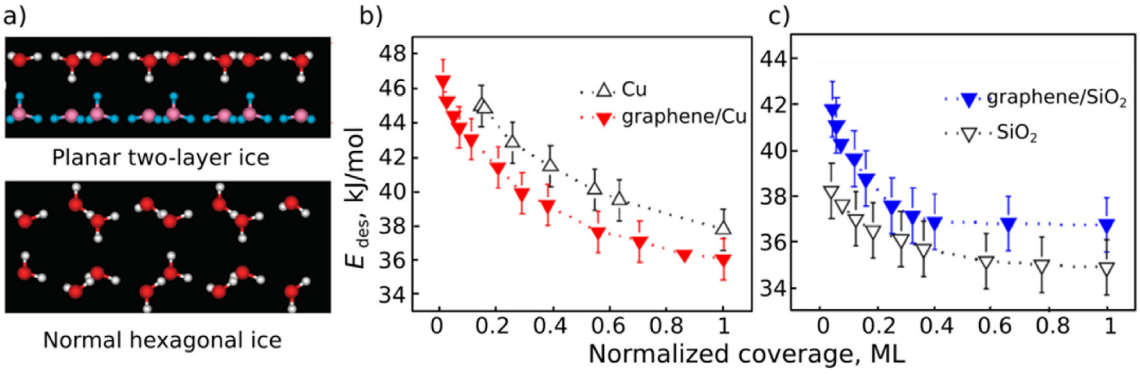

Fig. 5. Molecular adsorption on graphene or microscopic wettability of graphene under UHV. a) Calculated structures (side view) of the planar two-layers polymorph of water ice that forms on graphene (top) and normal three-dimensional hexagonal water ice (bottom) [25]. b) Desorption energy (E_{des}) as a function of benzene coverage (with ML depicting the number of benzene monolayers desorbed from the surface) for desorption of benzene from bare copper and graphene-on-copper [89]. c) Desorption energy (E_{des}) as a function of benzene coverage (ML – number of benzene monolayers desorbed from the surface) for desorption of benzene from bare SiO_2 and graphene-on-SiO_2 [89].

the expense of their weakening), as opposed to normal puckered three dimensional (3D) hexagonal ice (Fig. 5a) [25,27]. Although this phenomenon was previously predicted as a result of the confinement of water between two hydrophobic surfaces [94,95], the low energy electron diffraction, reflection–absorption infrared spectroscopy and rare-gas adsorption/desorption measurements showed that the surface of graphene actuates the unusual planar ordering of water molecules without any confinement. All other adsorbates (except benzene) manifested zero order kinetics desorption from graphene-on-platinum (111), indicating formation of the islands of condensed adsorbate in equilibrium with individual adsorbate molecules [27,29,96]. In contrast, benzene showed a first order kinetics at submonolayer coverages on graphene-on-platinum (111), which transitions to zero order for the second and subsequent adsorbed layers, indicating that island formation (i.e. when the adsorbate forms multilayer islands instead of continuous monolayer) is unfavourable for aromatic molecules due to the weaker adsorbate-adsorbate (compared to adsorbate-substrate) attractive interactions [30]. In that respect, benzene wets graphene on Pt(111) similarly to HOPG [97]. Methanol and ethanol, on one hand, have similar desorption energies on graphene and on HOPG, but on the other, presented a zero kinetic order on graphene, as opposed to the fractional kinetics orders on HOPG (0.26 and 0.08 respectively) [27,98,99].

By comparing the desorption characteristics of graphene on various substrates with those of the bare substrates, the substrate effect and the wetting transparency were assessed [31,89,90]. Interestingly, the transparency of graphene to desorption was shown to strongly depend on the adsorbate. Particularly, silicon and copper substrates strongly affect desorption of benzene [89], n-pentane [31], butane [90] and water [88] from graphene, even manifesting full transparency in the case of benzene (no data was presented for the desorption of n-pentane and butane from bare substrates thus no conclusion about wetting transparency in these cases could be made). The effect of the substrate on the microscopic wettability of graphene can be deduced as a difference between desorption energies of an adsorbate from graphene-on-a-substrate and from the bare substrate [31,89,90]. For example, the desorption energies and their coverage dependences of benzene on copper and on silicon were not affected by the graphene layer at all (Fig. 5b and c) [89]. Water, in contrast, exhibits different desorption characteristics (kinetic order and desorption energy) on substrates (namely, silicon and copper) with and without graphene layer [88]. Interestingly, graphene-coated SiO_2 appeared to be more hydrophilic than bare SiO_2, and graphene-coated copper appeared to be more hydrophobic than bare copper [88]. Also, a complex desorption behavior of graphene on ruthenium (0001) was reported: no transparency to the desorption of water [28] and benzene [26], but full transparency to desorption of n-butane [90]. These findings might be relevant to the fact that water intercalates and splits graphene on Ru(0001), as it was observed by STM [73].

Finally, the preparation and the quality of graphene samples must be taken into consideration in microscopic wettability studies as it is in the macroscopic contact angle measurements. In fact, graphene on Pt(111) and Ru(0001) were grown in situ in the UHV chamber, graphene on copper was grown using a CVD method and then mounted in the UHV chamber for desorption measurements, and graphene on SiO_2 was grown by CVD and then transferred using the PMMA-assisted method (with inevitably polymer residues adsorbed on the graphene surface). Certainly, graphene grown in situ in UHV on well-defined smooth and extremely clean metallic surfaces is expected to be of higher quality and to represent properties of a single layer of ideal (non-contaminated and free of bulk defects) graphene. Such samples, however, are only relevant to fundamental UHV studies, and there are no available contact angles for a comparative analysis. Samples which were exposed to air and underwent a transfer step (graphene on copper and SiO_2), on the other hand, are widely used and studied, but have structural defects and contamination, especially for graphene on SiO_2.

Overall, surface science methods allow probing the interactions between graphene and individual molecules in ultra-pure environments and quantification of the energy of desorption (which characterizes the strength of the interactions) and the kinetic order of desorption (indicates how the molecules pack on the graphene surface). However, correlating the interaction parameters of individual molecules in UHV with the macroscopic wettability of graphene in ambient atmosphere is not straightforward. Similarly to macroscopic measurements, inconsistencies associated with the sample preparation pose a real challenge for the interpretation and for the comparison between different sets of data, especially between microscopic (samples are prepared in UHV) and macroscopic (samples are exposed to air) studies. A systematic comparative analysis, which takes into consideration the effect of the sample preparation, is, therefore, needed.

6. Conclusions

Despite the contradictions still unresolved, the understanding of the wetting properties of graphene has come a long way. Fundamental dilemmas and technical difficulties arising from such a seemingly trivial question triggered tremendous effort of materials scientists and related communities. Clearly, unlike in bulk materials, simplified concepts such as hydrophilicity or wetting transparency cannot describe the variety of phenomena occurring in graphene and other 2D materials. Analysis of wettability studies of graphene, including macroscopic and microscopic measurements, yielded the conclusion that the apparent wettability of graphene is not only determined by the intrinsic properties of graphene, but also by the two media on each side of graphene]. Moreover, even the physical state of the matter is of crucial importance – solids, liquids and individual molecules have different effects on the electronic structure and morphology of graphene layer.

Graphene and two dimensional materials in general, require special theoretical considerations for the understanding of their behavior at different interfaces and under different conditions, and stimulated the development of unconventional experimental tools and designs for probing them. Ultimately, the findings and the tools developed for probing the wettability of graphene brought new insights to other areas of graphene research and made possible a step forward to more accessible and efficient graphene-based technologies.

Acknowledgements

The work leading to this review has gratefully received funding from the European Research Council under the European Union's Seventh Framework Programme (FP/2007–2013)/ERC Grant Agreement no. 335879 project acronym "Biographene" and the Netherlands Organization for Scientific Research (NWO-VIDI 723.013.007). The authors also thank Edgar Blokhuis for his valuable comments on the manuscript.

References

[1] P.G. de Gennes, Rev. Mod. Phys. 57 (1985) 827–863.
[2] D. Bonn, J. Eggers, J. Indekeu, J. Meunier, E. Rolley, Rev. Mod. Phys. 81 (2009) 739–805.
[3] L.A. Belyaeva, P.M.G. van Deursen, K.I. Barbetsea, G.F. Schneider, Adv. Mater. 30 (2018) 1–7.
[4] A. V Prydatko, L.A. Belyaeva, L. Jiang, L.M.C. Lima, G.F. Schneider, Nat. Commun. 9 (2018) 4185.

[5] O. Leenaerts, B. Partoens, F.M. Peeters, Phys. Rev. B 79 (2009) 235440.
[6] B. Bera, N. Shahidzadeh, H. Mishra, L.A. Belyaeva, G.F. Schneider, D. Bonn, Appl. Phys. Lett. 112 (2018) 1–6.
[7] F. Taherian, V. Marcon, N.F.A. Van Der Vegt, F. Leroy, Langmuir 29 (2013) 1457–1465.
[8] R. Raj, S.C. Maroo, E.N. Wang, Nano Lett. 13 (2013) 1509–1515.
[9] N. Akhtar, G. Anemone, D. Farias, B. Holst, Carbon N. Y. 141 (2019) 451–456.
[10] J. Rafiee, X. Mi, H. Gullapalli, A.V. Thomas, F. Yavari, Y. Shi, P.M. Ajayan, N.A. Koratkar, Nat. Mater. 11 (2012) 217–222.
[11] J. Driskill, D. Vanzo, D. Bratko, A. Luzar, J. Chem. Phys. 141 (2014) 18C517.
[12] C.J. Shih, Q.H. Wang, S. Lin, K.C. Park, Z. Jin, M.S. Strano, D. Blankschtein, Phys. Rev. Lett. 109 (2012) 176101.
[13] F. Du, J. Huang, H. Duan, C. Xiong, J. Wang, Appl. Surf. Sci. 454 (2018) 249–255.
[14] Q.H. Wang, Z. Jin, K.K. Kim, A.J. Hilmer, G.L.C. Paulus, C.-J. Shih, M.-H. Ham, J.D. Sanchez-Yamagishi, K. Watanabe, T. Taniguchi, J. Kong, P. Jarillo-Herrero, M.S. Strano, Nat. Chem. 4 (2012) 724–732.
[15] A. Kozbial, Z. Li, C. Conaway, R. McGinley, S. Dhingra, V. Vahdat, F. Zhou, B. D'Urso, H. Liu, L. Li, Langmuir 30 (2014) 8598–8606.
[16] D. Kim, N.M. Pugno, M.J. Buehler, S. Ryu, Sci. Rep. 5 (2015) 15526.
[17] Y.J. Shin, Y. Wang, H. Huang, G. Kalon, A.T.S. Wee, Z. Shen, C.S. Bhatia, H. Yang, Langmuir 26 (2010) 3798–3802.
[18] J. Liu, C.-Y. Lai, Y.-Y. Zhang, M. Chiesa, S.T. Pantelides, RSC Adv. 8 (2018) 16918–16926.
[19] G. Hong, Y. Han, T.M. Schutzius, Y. Wang, Y. Pan, M. Hu, J. Jie, C.S. Sharma, U. Müller, D. Poulikakos, Nano Lett. 16 (2016) 4447–4453.
[20] A. Ashraf, Y. Wu, M.C. Wang, K. Yong, T. Sun, Y. Jing, R.T. Haasch, N.R. Aluru, S. Nam, Nano Lett. 16 (2016) 4708–4712.
[21] S.S. Shams, R. Zhang, J. Zhu, Mater. Sci. 33 (2015) 566–578.
[22] H.C. Lee, W.-W. Liu, S.-P. Chai, A.R. Mohamed, A. Aziz, C.-S. Khe, N.M.S. Hidayah, U. Hashim, RSC Adv. 7 (2017) 15644–15693.
[23] M. Chen, R.C. Haddon, R. Yan, E. Bekyarova, Mater. Horiz. 4 (2017) 1054–1063.
[24] Z. Li, Y. Wang, A. Kozbial, G. Shenoy, F. Zhou, R. McGinley, P. Ireland, B. Morganstein, A. Kunkel, S.P. Surwade, L. Li, H. Liu, Nat. Mater. 12 (2013) 925–931.
[25] G.A. Kimmel, J. Matthiesen, M. Baer, C.J. Mundy, N.G. Petrik, R.S. Smith, Z. Dohnálek, B.D. Kay, J. Am. Chem. Soc. 131 (2009) 12838–12844.
[26] A. Chakradhar, K. Trettel, U. Burghaus, Chem. Phys. Lett. 590 (2013) 146–152.
[27] R.S. Smith, J. Matthiesen, B.D. Kay, J. Phys. Chem. A 118 (2014) 8242–8250.
[28] A. Chakradhar, U. Burghaus, Chem. Commun. 50 (2014) 7698–7701.
[29] R.S. Smith, R.A. May, B.D. Kay, J. Phys. Chem. B 120 (2016) 1979–1987.
[30] R.S. Smith, B.D. Kay, J. Phys. Chem. B 122 (2018) 587–594.
[31] N. Sivapragasam, M.T. Nayakasinghe, A. Chakradhar, U. Burghaus, J. Vac. Sci. Technol. A 35 (2017) 61404.
[32] S. Wang, Y. Zhang, N. Abidi, L. Cabrales, Langmuir 25 (2009) 11078–11081.
[33] C.D. van Engers, N.E.A. Cousens, V. Babenko, J. Britton, B. Zappone, N. Grobert, S. Perkin, Nano Lett. 17 (2017) 3815–3821.
[34] R. Su, X. Zhang, J. Therm. Sci. 27 (2018) 359–363.
[35] L. Spanu, S. Sorella, G. Galli, Phys. Rev. Lett. 103 (2009) 196401.
[36] T. Björkman, A. Gulans, A. V Krasheninnikov, R.M. Nieminen, Phys. Rev. Lett. 108 (2012) 235502.
[37] C.J. Van Oss, M.J. Roberts, R.J. Good, M.K. Chaudhury, Colloid. Surface. 23 (1987) 369–373.
[38] F.M. Fowkes, Ind. Eng. Chem. 56 (1964) 40–52.
[39] D.K. Owens, R.C. Wendt, J. Appl. Polym. Sci. 13 (1969) 1741–1747.
[40] D. Li, A.W. Neumann, J. Colloid Interface Sci. 148 (1992) 190–200.
[41] D. Li, A.W. Neumann, Langmuir 9 (1993) 50–54.
[42] A.W. Neumann, R.J. Good, C.J. Hope, M. Sejpal, J. Colloid Interface Sci. 49 (1974) 291–304.
[43] M. Annamalai, K. Gopinadhan, S.A. Han, S. Saha, H.J. Park, E.B. Cho, B. Kumar, A. Patra, S.-W. Kim, T. Venkatesan, Nanoscale 8 (2016) 5764–5770.
[44] J.-Y. Lu, T. Olukan, S.R. Tamalampudi, A. Al-Hagri, C.-Y. Lai, M. Ali Al Mahri, H. Apostoleris, I. Almansouri, M. Chiesa, Nanoscale 11 (2019) 7944–7951.
[45] Z. Li, A. Kozbial, N. Nioradze, D. Parobek, G.J. Shenoy, M. Salim, S. Amemiya, L. Li, H. Liu, ACS Nano 10 (2016) 349–359.
[46] A.I. Aria, P.R. Kidambi, R.S. Weatherup, L. Xiao, J.A. Williams, S. Hofmann, J. Phys. Chem. C 120 (2016) 2215–2224.
[47] J. Zhang, L. Lin, L. Sun, Y. Huang, A.L. Koh, W. Dang, J. Yin, M. Wang, C. Tan, T. Li, Z. Tan, Z. Liu, H. Peng, Adv. Mater. 29 (2017) 1700639.
[49] T. Ondarçuhu, V. Thomas, M. Nuñez, E. Dujardin, A. Rahman, C.T. Black, A. Checco, Sci. Rep. 6 (2016) 24237.
[50] G. Scocchi, D. Sergi, C. D'Angelo, A. Ortona, Phys. Rev. E 84 (2011) 61602.
[51] J.E. Andrews, S. Sinha, P.W. Chung, S. Das, Phys. Chem. Chem. Phys. 18 (2016) 23482–23493.
[52] G. Yiapanis, A.J. Makarucha, J.S. Baldauf, M.T. Downton, Nanoscale 8 (2016) 19620–19628.
[53] M.E. Schrader, J. Phys. Chem. 79 (1975) 2508–2515.
[54] D. Martinez-Martin, R. Longuinhos, J.G. Izquierdo, A. Marele, S.S. Alexandre, M. Jaafar, J.M. Gómez-Rodríguez, L. Bañares, J.M. Soler, J. Gomez-Herrero, Carbon N. Y. 61 (2013) 33–39.
[55] M.L. Read, P.B. Morgan, J.M. Kelly, C. Maldonado-Codina, J. Biomater. Appl. 26 (2011) 85–99.
[56] M.C. Lin, T.V. Svitova, Optom. Vis. Sci. 87 (2010) 440–447.
[57] T.O. Wehling, A.I. Lichtenstein, M.I. Katsnelson, Appl. Phys. Lett. 93 (2008) 202110.
[58] S. Sengupta, N.S. Nichols, A. Del Maestro, V.N. Kotov, Phys. Rev. Lett. 120 (2018) 236802.
[59] A. Ashraf, Y. Wu, M.C. Wang, N.R. Aluru, S.A. Dastgheib, S. Nam, Langmuir 30 (2014) 12827–12836.
[60] C.A. Amadei, C.-Y. Lai, D. Heskes, M. Chiesa, J. Chem. Phys. 141 (2014) 84709.
[61] C.-Y. Lai, T.-C. Tang, C.A. Amadei, A.J. Marsden, A. Verdaguer, N. Wilson, M. Chiesa, Carbon N. Y. 80 (2014) 784–792.
[62] A. Kozbial, Z. Li, J. Sun, X. Gong, F. Zhou, Y. Wang, H. Xu, H. Liu, L. Li, Carbon N. Y. 74 (2014) 218–225.
[63] G. Cunge, D. Ferrah, C. Petit-Etienne, A. Davydova, H. Okuno, D. Kalita, V. Bouchiat, O. Renault, J. Appl. Phys. 118 (2015) 123302.
[64] S.S. Shams, R. Zhang, J. Zhu, Mater. Sci. 33 (2015) 566–578.
[65] Q. Yu, J. Lian, S. Siriponglert, H. Li, Y.P. Chen, S.-S. Pei, Appl. Phys. Lett. 93 (2008) 113103.
[66] L.G. De Arco, Y. Zhang, A. Kumar, C. Zhou, IEEE Trans. Nanotechnol. 8 (2009) 135–138.
[67] A. Reina, X. Jia, J. Ho, D. Nezich, H. Son, V. Bulovic, M.S. Dresselhaus, J. Kong, Nano Lett. 9 (2009) 30–35.
[68] K.S. Kim, Y. Zhao, H. Jang, S.Y. Lee, J.M. Kim, K.S. Kim, J.-H. Ahn, P. Kim, J.-Y. Choi, B.H. Hong, Nature 457 (2009) 706–710.
[69] X. Li, W. Cai, J. An, S. Kim, J. Nah, D. Yang, R. Piner, A. Velamakanni, I. Jung, E. Tutuc, S.K. Banerjee, L. Colombo, R.S. Ruoff, Science 324 (2009) 1312–1314.
[70] Y. Zhang, L. Zhang, C. Zhou, Acc. Chem. Res. 46 (2013) 2329–2339.
[71] H.C. Lee, W.-W. Liu, S.-P. Chai, A.R. Mohamed, C.W. Lai, C.-S. Khe, C.H. Voon, U. Hashim, N.M.S. Hidayah, Procedia Chem. 19 (2016) 916–921.
[72] R. Xue, I. Abidi, Z. Luo, Funct. Mater. Lett. 10 (2017) 1730003.
[73] X. Feng, S. Maier, M. Salmeron, J. Am. Chem. Soc. 134 (2012) 5662–5668.
[74] J.E. Andrews, Y. Wang, S. Sinha, P.W. Chung, S. Das, Nano Lett. 19 (2018) 27421–27434.
[75] Y. Wang, S. Sinha, L. Hu, S. Das, Nano Lett. 5 (2017) 3815–3821.
[76] L.A. Belyaeva, W. Fu, H. Arjmandi-Tash, G.F. Schneider, ACS Cent. Sci. 2 (2016) 904–909.
[77] T. Hallam, N.C. Berner, C. Yim, G.S. Duesberg, Adv. Mater. Interf. 1 (2014) 1400115.
[79] Y. Su, H.-L. Han, Q. Cai, Q. Wu, M. Xie, D. Chen, B. Geng, Y. Zhang, F. Wang, Y.R. Shen, C. Tian, Nano Lett. 15 (2015) 6501–6505.
[80] Y. Han, L. Zhang, X. Zhang, K. Ruan, L. Cui, Y. Wang, L. Liao, Z. Wang, J. Jie, J. Mater. Chem. C 2 (2014) 201–207.
[81] K. Kumar, Y.-S. Kim, E.-H. Yang, Carbon N. Y. 65 (2013) 35–45.
[82] W.-H. Lin, T.-H. Chen, J.-K. Chang, J.-I. Taur, Y.-Y. Lo, W.-L. Lee, C.-S. Chang, W.-B. Su, C.-I. Wu, ACS Nano 8 (2014) 1784–1791.
[83] G. Zhang, A.G. Güell, P.M. Kirkman, R.A. Lazenby, T.S. Miller, P.R. Unwin, ACS Appl. Mater. Interfaces 8 (2016) 8008–8016.
[84] H. Park, I.-J. Park, D.Y. Jung, K.J. Lee, S.Y. Yang, Sung-Yool, 2D Mater. 3 (2016) 21003.
[85] I. Pasternak, A. Krajewska, K. Grodecki, I. Jozwik-Biala, K. Sobczak, W. Strupinski, AIP Adv. 4 (2014) 97133.
[86] L.M.C. Lima, H. Arjmandi-Tash, G.F. Schneider, ACS Appl. Mater. Interfaces 10 (2018) 11328–11332.
[87] H. Arjmandi-Tash, L. Jiang, G.F. Schneider, Carbon N. Y. 118 (2017) 556–560.
[88] A. Chakradhar, N. Sivapragasam, M.T. Nayakasinghe, U. Burghaus, Chem. Commun. 51 (2015) 11463–11466.
[89] A. Chakradhar, N. Sivapragasam, M.T. Nayakasinghe, U. Burghaus, J. Vac. Sci. Technol. A Vac. Surf. Film. 34 (2016) 21402.
[90] N. Sivapragasam, M.T. Nayakasinghe, U. Burghaus, J. Vac. Sci. Technol. A 34 (2016) 41404.
[91] D.A. King, Surf. Sci. 47 (1975) 384–402.
[92] S.T. Ceyer, Science 249 (1990) 133–139.
[93] H. Ulbricht, R. Zacharia, N. Cindir, T. Hertel, Carbon N. Y. 44 (2006) 2931–2942.
[94] R. Zangi, J. Phys. Condens. Matter 16 (2004) S5371.
[95] N. Giovambattista, P.J. Rossky, P.G. Debenedetti, Phys. Rev. Lett. 102 (2009) 50603.
[96] J.L. Daschbach, B.M. Peden, R.S. Smith, B.D. Kay, J. Chem. Phys. 120 (2004) 1516–1523.
[97] H. Ulbricht, R. Zacharia, N. Cindir, T. Hertel, Carbon N. Y. 44 (2006) 2931–2942.
[98] W.A. Brown, A.S. Bolina, Mon. Not. Roy. Astron. Soc. 374 (2007) 1006–1014.
[99] A.S. Bolina, A.J. Wolff, W.A. Brown, J. Phys. Chem. B 109 (2005) 16836–16845.